JCTC Journal of Chemical Theory and Computation

Article

pubs.acs.org/JCTC

Calculating the Bimolecular Rate of Protein−Protein Association with Interacting Crowders

Eng-Hui Yap[†,§,⊥] and Teresa Head-Gordon*[,†,‡,§,∥]

[†]UCSF and UC Berkeley Joint Graduate Group in Bioengineering, [‡]Department of Chemistry, [§]Department of Bioengineering, and [∥]Department of Chemical and Biomolecular Engineering, University of California, Berkeley, California 94720, United States

Supporting Information

ABSTRACT: We have recently introduced a method termed Poisson−Boltzmann semianalytical method (PB-SAM) for solving the linearized Poisson−Boltzmann equation for large numbers of arbitrarily shaped dielectric cavities with controlled precision. In this work we extend the applicability of the PB-SAM approach by deriving force and torque expressions that fully account for mutual polarization in both the zero- and first-order derivatives of the surface charges, that can now be embedded into a Brownian dynamics scheme to look at electrostatic-driven mesoscale assembly and kinetics. We demonstrate the capabilities of the PB-SAM approach by simulating the protein concentration effects on the bimolecular rate of association of barnase and barstar, under periodic boundary conditions and evaluated through mean first passage times. We apply PB-SAM to the pseudo-first-order reaction rate conditions in which either barnase or barstar are in great excess relative to the other protein (124:1). This can be considered a specific case in which the PB-SAM approach can be applied to crowding conditions in which crowders are not inert but can form interactions with other molecules.

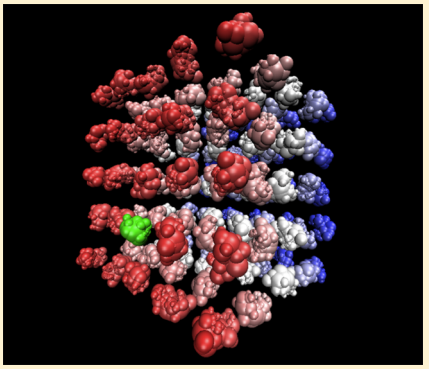

1. INTRODUCTION

The formation of protein−protein interactions is required for such diverse cellular processes as signaling, metabolic regulation, and motility. The ability to understand and control the mechanism of protein complex formation and the rate of association are all needed for understanding function, especially in the cellular milieu which gives rise to crowding effects.[1−4] Therefore the development of new models and algorithms for protein−protein complex formation kinetics under *in vivo* conditions of crowding is a central problem in computational biology.

Since electrostatic forces often orchestrate the earliest of recognition events for biomolecular complex formation, a realistic complexation study must include an accurate treatment of bulk electrolytes. This can be modeled using continuum mean-field theory with the Poisson−Boltzmann (PB) equation, which under low field condition be further simplified to the linearized Poisson−Boltzmann equation (LPBE). Various analytical and numerical treatments can be used to solve the LPBE.[5] Analytical methods typically allow rapid solution of the LPBE under specialized geometries such as spheres or cylinders.[6−12] Our group has achieved a fundamental result in deriving the first completely general analytical solution to the LPBE for computing the full *mutual* polarization and screened (salty) electrostatic interaction between arbitrary numbers of spheres of arbitrarily complex charge distributions, separated by arbitrary distance or concentration.[12]

In contrast, numerical methods (see ref 5 for a recent survey) such as finite-difference (FD)[13−15] and finite-element (FE)[16−18] methods can handle arbitrary dielectric boundaries by solving for the PB potential on a 3-D grid or mesh. Recent theoretical advances have addressed some of the critical limitations in traditional FE and FD formulations: charge singularities[19−21] were mitigated, and electric displacement continuity was enforced across dielectric boundaries using matched-interface techniques.[22,23] However, analytical formulations of forces, as derived by Gilson[24] and Im et al.,[25] are based on one single macromolecule, and therefore do not account for mutual polarization effects of the *gradient* due to movement of one macromolecule with respect to another. To correctly account for mutual gradient polarization in the FD or FE context, one could employ the 'virtual work' approach,[26] whereby the electrostatic energy is recalculated after a small displacement in the x, y, and z direction, respectively, and the force in each direction given by the difference in energy over the displaced distance. Even with the assumption of rigid macromolecules, this would still require four finite difference computations for each macromolecule, making it computationally laborious. Most importantly, the requirement that the solution be solved on a grid limits its practical application to spatial domains of either two to three typical macromolecules at reasonably high resolution (∼0.2 Å) or to larger numbers of macromolecules with greatly diminished resolution (∼2.0−5.0 Å) and thus solution accuracy, rendering them unsuitable for long length scale association simulations.

Received: January 19, 2013
Published: March 14, 2013

ACS Publications © 2013 American Chemical Society

Boundary element (BE) methods[27−31] are an attractive alternative since they satisfy both the Dirichlet and von Neuman boundary conditions by construction, singular charges can be correctly treated, and most importantly the 2D solutions on the macromolecular surface remove spatial resolution limitations imposed by the 3D grid of the FD or FE solvers. However increasing the number of boundary surface element results in an increasingly large dense matrix to be solved with severe memory requirements, a problem which scales with the number of macromolecules. Acceleration of the BE approach[28,32] incorporating fast multipole methods have rendered BE computational times comparable to state-of-the-art software packages like the Adaptive Poisson−Boltzmann Solver (APBS)[13] based on FD solutions. A recently available algorithm, AFMPB,[33] allows calculation of electrostatics energy and forces, but it has yet to be demonstrated to be efficient enough for dynamic simulation and only includes self-polarization effects.

We have previously presented a new numerical approach to solving the LPBE equation, Poisson−Boltzmann semianalytical method (PB-SAM), that combines the advantages of both the boundary element and our analytical formalism,[12] by representing a molecule as a collection of overlapping spheres.[34] We showed that PB-SAM converges to the analytical solution with better accuracy and at greatly reduced cost relative to the readily available public domain PB solver APBS.[13] In this work we extend our PB-SAM approach[34] by deriving expressions for force and torque that handle complete *mutual* polarization effects.

To demonstrate the power of the PB-SAM approach, we apply our new LPBE algorithm to study the bimolecular association of the ribonuclease barnase and its intracellular inhibitor, barstar, under conditions of crowding. Barnase/barstar association is a classic example of electrostatically steered diffusion-limited association. The association kinetics has been extensively characterized, both experimentally[35] and computationally[36,37] using the Northrup-Allison-McCammon (NAM) method;[38] in the earlier computational study the electrostatics were modeled using effective charges, which accounts for self-polarization but not mutual polarization. The NAM method is based on the Smoluchowski equation,[38] and its underlying assumption is that the mobile molecule B only experiences isocentric forces from a stationary molecule A, i.e. concentration effects that modulate intraspecies interactions A:A and B:B as per crowding are not taken into account. A potentially more powerful rate constant calculation method would take these intraspecies *interaction* into account, beyond the excluded volume effect typically modeled under crowding conditions; however, it demands an efficient algorithm capable of computing the electrostatic forces and torques for multiple molecules on the fly. Because the PB-SAM method enables the calculation of full mutual polarization effects in systems of hitherto inaccessible spatial dimensions, it thereby allows the calculation of kinetic parameters of rate equations which can in turn be inputs to chemical master equations or stochastic simulations.

The paper is organized as follows. In Section 2 we review the PB-SAM formalism and introduce for the first time the force and torque expressions for our new LPBE solver. We also provide the necessary detail of the Brownian dynamics simulations and the molecular models of barnase and barstar. In Section 3 we compare the results of the bimolecular rate of association of a single barnase and barstar calculated using NAM and that calculated from a multimolecular PB-SAM simulation in which there is an excess concentration of either barnase and barstar, to evaluate a pseudo-first-order rate constant derived from mean first passage times of a docked complex. We ignore hydrodynamic interactions which is almost certainly important for these type of rate calculations and could potentially limit a quantitative connection to experiments performed on barnase-barstar under crowding conditions.[4] We emphasize that the purpose of our work here is to present new PBE methodology and the ability, for example, to represent crowding agents with more complex and realistic interaction potentials. Section 4 provides our conclusions on the PB-SAM method and the outcome of our rate study which finds only a ∼30% rate enhancement on barnase-barstar association rates, in agreement with experiment.[4]

2. THEORY

The method for solving mutually polarized charge distribution has been previously presented in ref 34. Here we first summarize the principal result, namely the solution of the charge distribution due to mutual polarization, followed by derivation of expressions for force and torque. Further details are given in the Supporting Information.

Solution of Mutually Polarized Charge Distribution. The system of interest comprises of N_{mol} macromolecules immersed in an implicit aqueous salty solvent. Each macromolecule I is represented as a collection of $N_S^{(I)}$ overlapping spheres with dielectric constant ε_{in} and embedded with $N_C^{(I)}$ fixed partial charges. The solvent is treated as a continuum with dielectric constant ε_{out}. Screening effects due to mobile ions are modeled via the inverse Debye length κ. The linearized PB equation (LPBE) gives the potential Φ at any point $\mathbf{r}$ in space $\mathcal{R}^3$ in e.s.u-c.g.s. convention as

$$-\nabla[\varepsilon(\mathbf{r})\nabla\Phi(\mathbf{r})] + \kappa^2\Phi(\mathbf{r}) = 4\pi\rho_{fixed}(\mathbf{r}) \tag{1}$$

where $\varepsilon(\mathbf{r})$ is the relative dielectric function, ρ_{fixed} is the charge density due to the fixed protein partial charges, and $\kappa = (8\pi\bar{n}e^2/\varepsilon_{out}k_BT)^{1/2}$, where $\bar{n}$ is the bulk concentration of monovalent salt in the solution, e is the fundamental electronic charge, k_B is the Boltzmann constant, and T is the absolute temperature.

The potentials inside and outside a molecule I are given respectively by

$$\Phi_{out}(\mathbf{r}) = \sum_{I=1}^{N_{mol}} \left(\frac{1}{4\pi} \int_{d\Omega^{(I)}} \frac{e^{-\kappa|\mathbf{r}-\mathbf{r}'|}}{|\mathbf{r}-\mathbf{r}'|} h^{(I)}(\mathbf{r}')d\mathbf{r}' \right) \tag{2a}$$

$$\Phi_{in}^{(I)}(\mathbf{r}) = \sum_{\alpha=1}^{N_C^{(I)}} \frac{1}{|\mathbf{r}-\mathbf{r}_\alpha^{(i)}|} \frac{q_\alpha^{(I)}}{\varepsilon_{in}} + \frac{1}{4\pi} \int_{d\Omega^{(I)}} \frac{1}{|\mathbf{r}-\mathbf{r}'|} f^{(I)}(\mathbf{r}')d\mathbf{r}' \tag{2b}$$

where $f(\mathbf{r})$ and $h(\mathbf{r})$ are the *reactive* and *effective* surface charge distributions, respectively. The charge distribution on sphere k, denoted as $f^{(I,k)}(\mathbf{r})$ and $h^{(I,k)}(\mathbf{r})$, can be transformed into *reactive* and *effective* multipoles:

$$F_{nm}^{(I,k)} \equiv \frac{1}{4\pi} \int_{d\Omega^{(I,k)}} f^{(I,k)}(\mathbf{r}') \left(\frac{a^{(I,k)}}{r'} \right)^{n+1} \overline{Y_{nm}^{(I,k)}}(\theta', \phi')d\mathbf{r}' \tag{3a}$$

$$H_{nm}^{(I,k)} \equiv \frac{1}{4\pi} \int_{d\Omega^{(i,k)}} h^{(I,k)}(\mathbf{r}') \left(\frac{r'}{a^{(I,k)}} \right)^{n} \hat{i}_n(\kappa r') \overline{Y_{nm}^{(I,k)}}(\theta', \phi')d\mathbf{r}' \tag{3b}$$

where $a^{(I,k)}$ is the radius of sphere (I,k), and (used later in eqs 12a−12b) are adapted modified spherical Bessel functions of the first and second kind[12] respectively. Coefficients of $\boldsymbol{F}^{(I,k)}$ and $\boldsymbol{H}^{(I,k)}$ can then be solved iteratively using

$$F_{nm}^{(I,k)} = \langle \mathbf{I}_{E,nm}^{(I,k)}, \mathbf{WF}^{(I,k)} \rangle \tag{4a}$$

$$\frac{H_{nm}^{(I,k)}}{\hat{i}_n(\kappa a^{(I,k)})} = \langle \mathbf{I}_{E,nm}^{(I,k)}, \mathbf{WH}_H^{(I,k)} \rangle \tag{4b}$$

where $\langle\ \rangle$ denotes an inner product, and $\boldsymbol{WF}^{(k,I)}$ and $\boldsymbol{WH}^{(k,I)}$ are scaled multipoles computed from fixed charges and polarization charges from other spheres (see Supporting Information Eqns S1.1a-b), and $\boldsymbol{I}_E^{(I,k)}$ is a matrix of surface integrals over the exposed surface, defined by

$$\mathbf{I}_{E,lsnm}^{(I,k)} \equiv \frac{1}{4\pi} \int_{\phi_E} \int_{\theta_E} Y_{ls}^{(I,k)}(\theta', \phi') \overline{Y_{nm}^{(I,k)}}(\theta', \phi') \sin\theta' d\theta' d\phi' \tag{5}$$

The above surface integral is evaluated once before the simulation, using the quadrature method with each sphere discretized uniformly into 72,000 spiral grid points using the method of Rakhmanov.[39]

The interaction energy of sphere k is the inner product of its effective multipole $\boldsymbol{H}^{(I,k)}$ with its local expansion of external (i.e., intermolecular) effective charges, $\boldsymbol{LHN}^{(I,k)}$. The total interaction energy of molecule I is in turn the sum of interaction energies of all constituent spheres

$$\begin{aligned} W^{(I)} &= \sum_{k=1}^{N_S^{(I)}} \langle \mathbf{LHN}^{(I,k)}, \mathbf{H}^{(I,k)} \rangle \\ &= \sum_{k=1}^{N_S^{(I)}} \sum_{n=0}^{p} \sum_{m=-n}^{n} LHN_{nm}^{(I,k)} \overline{H}_{nm}^{(I,k)} \end{aligned} \tag{6}$$

Force on an Effective Charge. The surface of each sphere can be discretized into M_P grid points, of which M_E are exposed and M_B are buried. We only need to consider the force experienced at each exposed grid point P, since buried grid points have no surface charge and hence experience no force. We begin by deriving an expression for the force at P and then summing up contributions from all exposed charges to derive the total force and torque on molecule I. We only consider forces due to external field, because forces due to intramolecular effective charges cancel out and do not contribute to the overall force and torque on molecule I.

We shall use the shorthand h_P to denote $h(\boldsymbol{r}_P)$, the effective charge at sphere point P. The multipole coefficient $\mathbf{H}_P^{(I,k)}$ is the product of h_P and the spherical harmonic $\mathbf{Y}_P^{(I,k)} \equiv \mathbf{Y}^{(I,k)}(\theta_P,\varphi_P)$. The force $\mathbf{f}_P$ acting on the effective charge at point P is the negative gradient of the interaction energy of charge h_P with the external field:

$$\begin{aligned} \mathbf{f}_P &= -\nabla_P W_P = -\nabla_P \langle \mathbf{LHN}^{(I,k)}, \mathbf{H}_P^{(I,k)} \rangle \\ &= -\langle \nabla_P \mathbf{LHN}^{(I,k)}, \mathbf{H}_P^{(I,k)} \rangle - \langle \mathbf{LHN}^{(I,k)}, \nabla_P \mathbf{H}_P^{(I,k)} \rangle \\ &= -\langle \nabla_P \mathbf{LHN}^{(I,k)}, \mathbf{H}_P^{(I,k)} \rangle - \langle \mathbf{LHN}^{(I,k)}, \nabla_P h_P \cdot \mathbf{Y}_P^{(I,k)} \rangle \\ &\quad - \langle \mathbf{LHN}^{(I,k)}, h_P \cdot \nabla_P \mathbf{Y}_P^{(I,k)} \rangle \end{aligned} \tag{7}$$

In rigid body dynamics, the translational force on a molecule acting through its center of mass is the sum of all forces acting on all its constituent parts. Summing up $\mathbf{f}_P$ from eq 7 from all exposed points, we get the translational force $\mathbf{f}_I$ on molecule I as

$$\mathbf{f}_I = \sum_{allP} \mathbf{f}_P = \sum_{k}^{Nk^{(I)}} \sum_{P \in k} \mathbf{f}_P \tag{8}$$

This can be expressed in terms of effective multipoles, local expansions, and their gradients under fixed orientation $\tilde{\nabla}_I$ (see the Supporting Information) as

$$\mathbf{f}_I = \sum_{k}^{Nk^{(I)}} \langle \tilde{\nabla}_I \mathbf{LHN}^{(I,k)}, \mathbf{H}^{(I,k)} \rangle + \langle \mathbf{LHN}^{(I,k)}, \tilde{\nabla}_I \mathbf{H}^{(I,k)} \rangle \tag{9}$$

Solution of Mutually Polarized Gradients. We now need to compute gradients $\tilde{\nabla}_I \mathbf{H}^{(I,k)}$ and $\tilde{\nabla}_I \mathbf{LHN}^{(I,k)}$, which account for how the position of molecule I changes the polarization charges. The gradient $\tilde{\nabla}_I \mathbf{LHN}^{(I,k)}$ is given by

$$\begin{aligned} \tilde{\nabla}_I \mathbf{LHN}^{(I,k)} &= \sum_{J \neq I} \sum_{j}^{N_S^{(J)}} \tilde{\nabla}_I \mathbf{T}_\kappa^{(I,k)(J,j)} \mathbf{H}^{(J,j)} \\ &\quad + \sum_{J \neq I} \sum_{j}^{N_S^{(J)}} \mathbf{T}_\kappa^{(I,k)(J,j)} \tilde{\nabla}_I \mathbf{H}^{(J,j)} \end{aligned} \tag{10}$$

where $\boldsymbol{T}_\kappa^{(I,k)(J,j)}$ denotes the multipole-to-local re-expansion operator from sphere (J,j) to sphere (I,k), with $\chi = 0$ for $J = I$ (intra-molecular re-expansion) and $\chi = \kappa$ for $J \neq I$ (inter-molecular re-expansion) (see the Supporting Information). The first sum can be computed from the converged solutions of effective multipoles $\boldsymbol{H}$ (eqs 4a−4b). For the second sum, we would need $\tilde{\nabla}_I \mathbf{H}^{(J,j)}$. That is, for each sphere, we need to compute the gradient of its effective multipole $\mathbf{H}$, with respect to *every* molecule I.

The gradient polarization step thus comprises of three nested iteration loops. The outermost loop goes over $1 \leq J \leq N_{mol}$ to compute gradients with respect to each J. The middle and innermost loops then solve for $\tilde{\nabla}_J \mathbf{H}^{(I,k)}$ of all spheres. Below we detailed the formulism for solving $\tilde{\nabla}_J \mathbf{H}^{(I,k)}$ for a sphere (I,k).

To compute $\tilde{\nabla}_J \mathbf{H}^{(I,k)}$ with respect to molecule J, we begin by applying the gradient operator $\tilde{\nabla}_J$ to eqs 4a and 4b:

$$\tilde{\nabla}_J F_{nm}^{(I,k)} = \langle I_{E,nm}^{(I,k)}, \tilde{\nabla}_J \mathbf{WF}^{(I,k)} \rangle \tag{11a}$$

$$\tilde{\nabla}_J \frac{H_{nm}^{(I,k)}}{\hat{i}_n(\kappa a^{(I,k)})} = \langle I_{E,nm}^{(I,k)}, \tilde{\nabla}_J \mathbf{WH}_H^{(I,k)} \rangle \tag{11b}$$

If molecule I is fixed in orientation, $\boldsymbol{I}_E$, $\boldsymbol{E}^{(I,k)}$, and $\boldsymbol{LE}^{(I,k)}$ do not depend on position of I since their positions move concertedly with I, so $\tilde{\nabla}_J \mathbf{WF}^{(I,k)}$ and $\tilde{\nabla}_J \mathbf{WH}^{(I,k)}$ can be simplified to

$$\begin{aligned} \tilde{\nabla}_J WF_{nm}^{(I,k)} &= e^{-\kappa a^{(I,k)}} [n\hat{k}_n(\kappa a^{(I,k)}) - (2n+1)\hat{k}_{n+1}(\kappa a^{(I,k)})] \tilde{\nabla}_J \\ &\quad \times H_{nm}^{(I,k)} + (2n+1-n\varepsilon) \tilde{\nabla}_J F_{nm}^{(I,k)} \\ &\quad + a^{(I,k)} \left[n\hat{i}_n(\kappa a^{(I,k)}) + \frac{(\kappa a^{(I,k)}) \hat{i}_{n+1}(\kappa a^{(I,k)})}{2n+3} \right] \tilde{\nabla}_J \\ &\quad \times (LH_{nm}^{(I,k)} + LHN_{nm}^{(I,k)}) - n\varepsilon a^{(I,k)} (\tilde{\nabla}_J LF_{nm}^{(I,k)}) \end{aligned} \tag{12a}$$

$$\tilde{\nabla}_J WH_{nm}^{(I,k)} = \left[\frac{2n+1}{\hat{i}_n(\kappa a^{(I,k)})} - e^{-\kappa a^{(I,k)}}\hat{k}_n(\kappa a^{(I,k)})\right]\tilde{\nabla}_J \times H_{nm}^{(I,k)} + \tilde{\nabla}_J F_{nm}^{(I,k)} + a^{(I,k)}\tilde{\nabla}_J LF_{nm}^{(I,k)} - a^{(I,k)}\hat{i}_n(\kappa a^{(I,k)})\tilde{\nabla}_J(LH_{nm}^{(I,k)} + LHN_{nm}^{(I,k)}) \quad (12b)$$

where $\varepsilon = \varepsilon_{in}/\varepsilon_{out}$.

During each middle-loop iteration, we consider one sphere (I,k) and compute the local expansions $\tilde{\nabla}_J\mathbf{LF}^{(I,k)}$, $\tilde{\nabla}_J\mathbf{LH}^{(I,k)}$, and $\tilde{\nabla}_J\mathbf{LHN}^{(I,k)}$ from outer spheres' polarized gradients. The local expansions are defined below:

$$\tilde{\nabla}_J\mathbf{LF}^{(I,k)} = \sum_{j\neq k}^{N_S^{(I)}} \mathbf{T}_0^{(I,k)(I,j)}\tilde{\nabla}_J\mathbf{F}^{(I,k)};$$

$$\tilde{\nabla}_J\mathbf{LH}^{(I,k)} = \sum_{j\neq k}^{N_S^{(I)}} \mathbf{T}_\kappa^{(I,k)(I,j)}\tilde{\nabla}_J\mathbf{H}^{(I,j)} \quad (13)$$

$$\tilde{\nabla}_J\mathbf{LHN}^{(I,k)} = \sum_{M\neq I}\sum_{m}^{N_S^{(M)}} \tilde{\nabla}_J\mathbf{T}_\kappa^{(I,k)(M,m)}\mathbf{H}^{(M,m)} + \sum_{M\neq I}\sum_{m}^{N_S^{(M)}} \mathbf{T}_\kappa^{(I,k)(M,m)}\tilde{\nabla}_J\mathbf{H}^{(M,m)} \quad (14)$$

Note that intramolecular re-expansions (within same molecule I) do not have a $\tilde{\nabla}_J\mathbf{T}\cdot\mathbf{H}$ component, since for intramolecular re-expansion the operation $\boldsymbol{T}$ does not change with the position of I. Finally, with all local expansions computed, we can enter the innermost loop to solve for $\tilde{\nabla}_J\mathbf{F}^{(I,k)}\tilde{\nabla}_J\mathbf{H}^{(I,k)}$ using eqs 11a-11b and 12a-12b.

Since mutual polarization is a short-range effect, a cutoff r_{cut} can be used during charge and gradient polarization to simplify the computations. *Intermolecular* spheres whose surface-to-surface distances are greater than r_{cut} will not be included in each other's external field. The validity of cutoffs for intramolecular spheres needs to be further investigated.

Expressions for Force and Torque. The translational force on molecule I is given

$$\mathbf{f}_I = -\sum_{k}^{Nk^{(I)}} \mathbf{f}_{I,k} \quad (15)$$

where

$$\mathbf{f}_{I,k} = -\langle\tilde{\nabla}_I\mathbf{LHN}^{(I,k)}, \mathbf{H}^{(I,k)}\rangle + \langle\mathbf{LHN}^{(I,k)}, \tilde{\nabla}_I\mathbf{H}^{(I,k)}\rangle \quad (16)$$

The torque on a charge at position P about the molecule I's center of mass $\boldsymbol{c}^{(I)}$ is given by the cross product of its position $\mathbf{r}_P^{(I)}$ with respect to $\boldsymbol{c}^{(I)}$ and the force it experienced, $\mathbf{f}_P$. The total torque on molecule I is then the sum of all torques:

$$\boldsymbol{\tau}_I = \sum_{k}^{Nk^{(I)}}\sum_{P\in k} \boldsymbol{\tau}_P = \sum_{k}^{Nk^{(I)}}\sum_{P\in k} \mathbf{r}_P^{(I)}\times\mathbf{f}_P \quad (17)$$

We can re-express $\mathbf{r}_P^{(I)}$ as the sum of vectors from center of molecule I to center of sphere k ($\mathbf{c}^{(I,k)}$) and from center of sphere k to point P ($\mathbf{r}_P^{(I,k)}$). The total torque about the center of molecule I is then

$$\boldsymbol{\tau}_I = \sum_{k}^{Nk^{(I)}} \mathbf{c}^{(I,k)}\times\mathbf{f}_k + \sum_{k}^{Nk^{(I)}}\sum_{P\in k} \mathbf{r}_P^{(I,k)}\times\mathbf{f}_P \quad (18)$$

where

$$\mathbf{f}_P = -\sum_{k}^{Nk^{(I)}} \langle\tilde{\nabla}_I\mathbf{LHN}^{(I,k)}, \mathbf{H}_P^{(I,k)}\rangle + \langle\mathbf{LHN}^{(I,k)}, \tilde{\nabla}_I\mathbf{H}_P^{(I,k)}\rangle \quad (19)$$

and

$$\mathbf{H}_P^{(I,k)} = h(\theta_P, \phi_P)\mathbf{Y}_{nm}^{(I,k)}(\theta_P, \phi_P) \quad (20a)$$

$$\tilde{\nabla}_J\mathbf{H}_{P,\alpha}^{(I,k)} = (\tilde{\nabla}_j h(\theta_P, \phi_P))_\alpha\mathbf{Y}_{nm}^{(I,k)}(\theta_P, \phi_P), \quad \alpha = x, y, z \quad (20b)$$

Equations 15-16 and equations 18-20b will be used to compute the force and torque respectively.

Brownian Dynamics. We have adopted the Brownian dynamics simulation protocol developed by Ermak and McCammon.[40] Each molecule I is treated as a Brownian particle experiencing a conservative force $\mathbf{f}_I$ and torque $\boldsymbol{\tau}_I$, in addition to friction and random force due to the solvent. Assuming no hydrodynamic interaction between the macromolecules, the displacement $\Delta\mathbf{r}_I$ and angular rotation $\Delta\boldsymbol{\vartheta}_I$ per time step Δt are given by

$$\Delta\mathbf{r}_I = \frac{D_{I,trans}\Delta t}{k_B T}\mathbf{f}_I + \mathbf{S}_I(\Delta t) \quad (21a)$$

$$\Delta\boldsymbol{\vartheta}_I = \frac{D_{I,rot}\Delta t}{k_B T}\boldsymbol{\tau}_I + \Theta_I(\Delta t) \quad (21b)$$

where the stochastic displacement (S) and rotation (Θ) have the properties

$$\langle S_\alpha\rangle = 0, \quad \langle S_\alpha{}^2\rangle = 2D_{I,trans}\Delta t \quad (22a)$$

$$\langle\Theta_\alpha\rangle = 0, \quad \langle\Theta_\alpha{}^2\rangle = 2D_{I,rot}\Delta t \quad \alpha = x, y, z \quad (22b)$$

where the index I runs over molecule $1 \le I \le N$. The translational and rotational diffusion constants of each molecule I are set to the values used in ref 36, with $D_{trans} = 0.015$ A^{2}ps^{-1} for both barnase and barstar, and $D_{rot} = 4.5\times10^{-5}$ for barnase and 4×10^{-5} for barstar. Each molecule I is moved in turn, first undergoing displacement $\Delta\mathbf{r}_I$, followed by rotation $\Delta\boldsymbol{\vartheta}_I$. Both displacement and rotation moves are checked for a collision, defined as when any sphere of molecule I overlaps with spheres of other molecules. If a collision occurs, a new stochastic displacement or rotation move is generated and checked, until a valid move is obtained.

Protein Models. The structure of barnase and barstar were taken from the PDB (code 1BRS).[41] Chain A was used for barnase, with the missing residues 1 and 2 modeled using CE alignment[42] of chain B onto chain A. Chain D was used for barstar. The pdb chains were converted into PQR format using pdb2pqr,[43,44] which assigned partial atomic charges using the AMBER 99 force field[45] and calculated protonation states at pH = 8.0 (the pH of the original experiment[35]) using PROPKA,[46] giving net charges of 2.0 and −5.0 for barnase and barstar respectively.

We then generated the solvent excluded molecular surface (SES) for each protein using MSMS,[47] with probe radius = 1.5 Å and a density of 3.0. The SES and PQR files were inputted

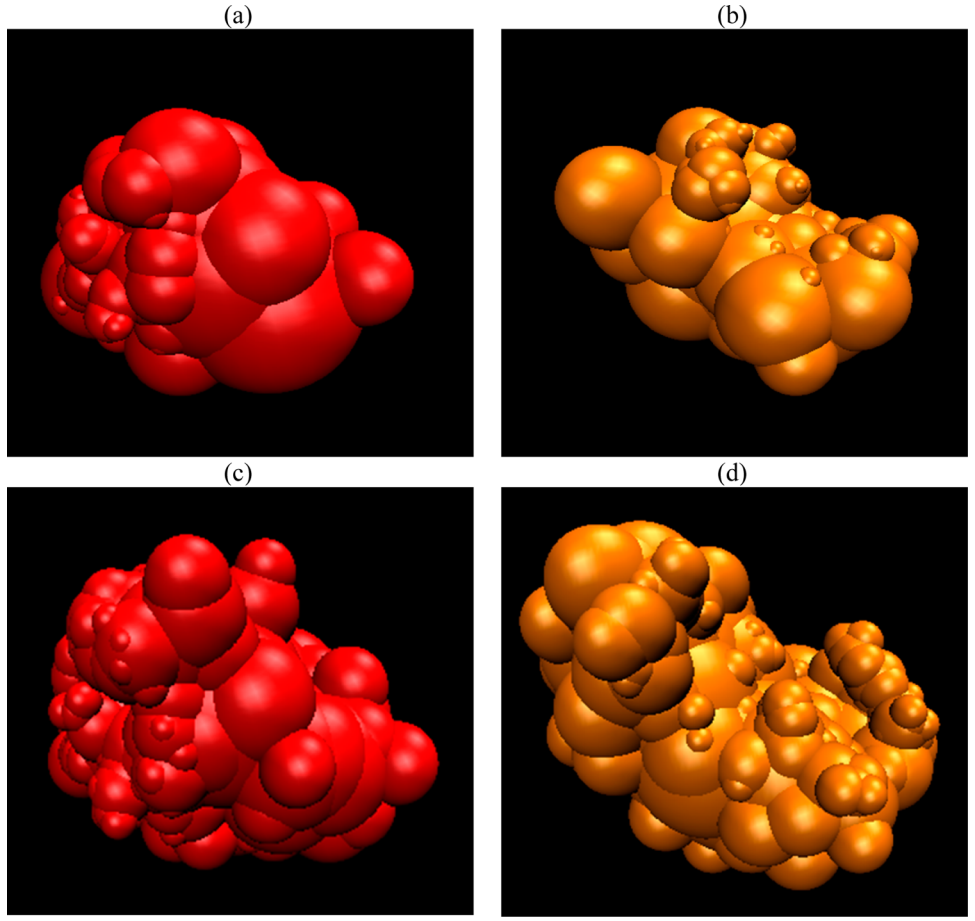

Figure 1. Surface representation of barnase and barstar under the PB-SAM model: (a) barnase and (b) barstar using discretization tolerance of 1.0 Å at the interface and 5.0 Å otherwise ('s5i1'); (c) barnase and (d) barstar using tolerance of 0.5 Å at the binding interface and 2 Å otherwise ('s2i0.5').

Table 1. Contact Sphere Pairs for Docking Criteria[a]

barnase				barstar				
sphere center				sphere center				
x	*y*	*z*	sphere radius [Å]	*x*	*y*	*z*	sphere radius [Å]	corresponding barnase:barstar contact-pair in ref 36
28.301	44.689	7.816	1.824	23.556	36.176	1.911	1.661	NH2 Arg-59: OE1 Glu-76
22.931	39.926	16.517	7.382	38.501	41.571	−3.117	8.670	O His-102: ND2 Asn-33
40.828	43.274	15.283	1.721	41.590	30.319	10.515	6.539	OE2 Glu-60: N Leu-34
25.166	27.428	7.651	2.827	30.876	43.257	−3.615	2.920	N Arg-59: OD1 Asp-35
30.219	46.397	8.927	1.487	29.514	34.511	−1.557	3.946	NZ Lys-27: OG1 Thr-42
26.671	32.092	10.255	1.487	30.991	44.349	3.364	3.917	O Arg-83: OH Tyr-29
37.158	42.422	20.865	5.717	24.716	37.671	2.256	2.769	NH2 Arg-83: OD1 Asp-39
37.158	42.422	20.865	5.717	28.561	43.730	4.147	1.824	NH1 Arg-83: O Gly-43

[a]Formation of encounter complex is defined as two or more contact sphere pairs having surface-to-surface distances within 3.5 Å.

into an in-house program to discretize the protein into spheres. At each iteration, the program uses a greedy Monte Carlo algorithm to search for a sphere center that encompasses the largest number of fixed partial charges. Charges within this sphere center were then removed, and the search was repeated with the remaining charges. A stipulated tolerance controls how far from the SES the sphere surface can protrude. We experimented with two sets of tolerance: (i) 0.5 Å at the binding interface and 2.0 Å otherwise ('s2i0.5′) and (ii) 1.0 Å at the interface and 5.0 Å otherwise ('s5i1'). Figure 1 shows the barnase-barstar docked complex under the s5i1 and s2i0.5 representations. We find that both representations permit docking to occur under similar docking criteria as that specified by Wade, hence the 's5i1' representation is sufficient for docking and was used in subsequent association studies.

The docking criteria we used was adopted from that specified by Gabdoulline and Wade,[36] whereby the encounter complex is defined in terms of residue contact pairs whose docking distances were fitted to reproduce Fersht's experimental results for wild-type and mutants of the barnase and barstar system. Given the list of eight hydrogen-bond forming atoms from ref 36 we identified the smallest spheres in the s5i1 representation that encompasses them ('contact-spheres', see Table 1). To be considered docked i.e. forming the reactive encounter complex, at least two contact-sphere pairs must have surface-to-surface distances within 3.5 Å. This distance translates approximately to

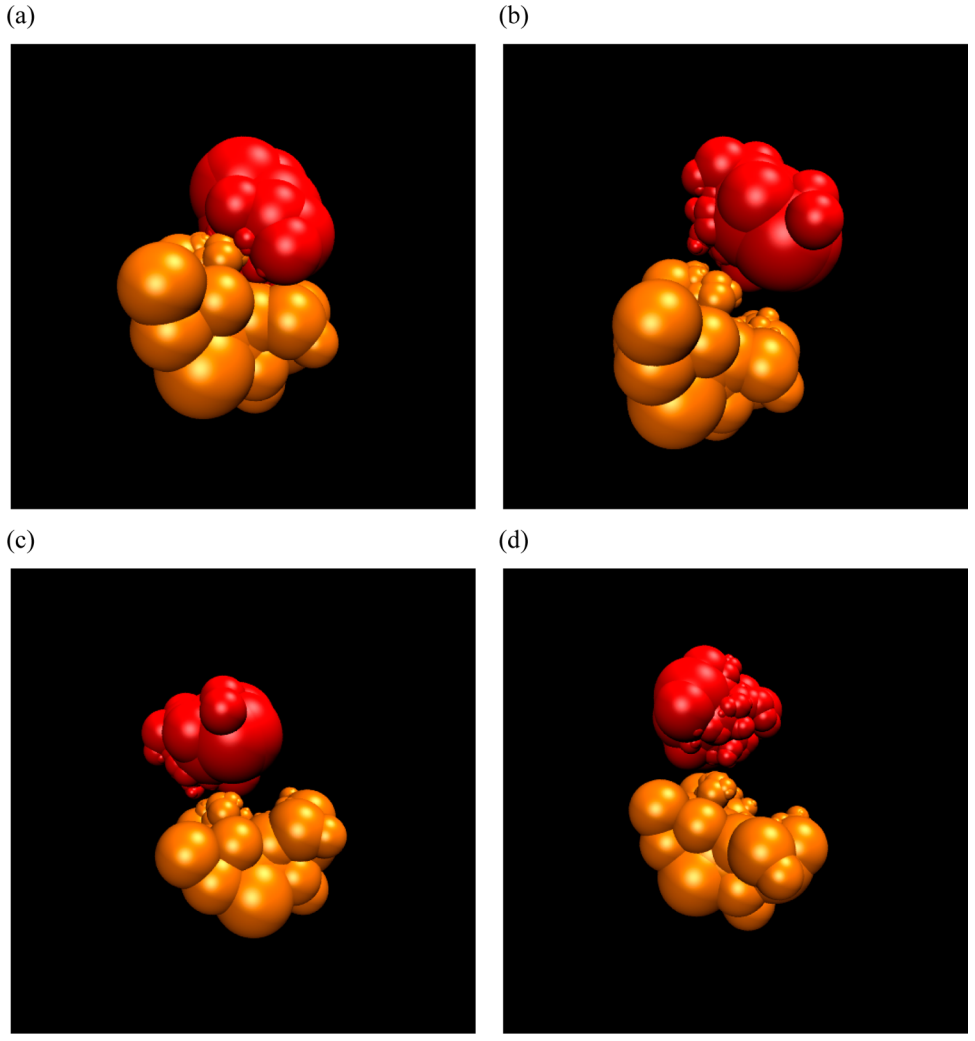

Figure 2. Docked barnase and barstar encounter complexes: (a) the docked complex (1BRS) of barnase (red) and barstar (orange) under the s5i1 representation; (b-d) representative encounter complexes under our docking criteria.

an atom-to-atom distance of 6.25 Å used by Wade. Figure 2 shows the docked complex of 1BRS rendered in our s5i1 discretized sphere presentation (Figure 2(a)) and representative snapshots of encounter complexes satisfying our docking criteria (Figures 2b-2d). We note that our adapted docking definition using s5i1 will not be exactly the same as an all-atom representation of barnase and barstar.

Simulation Parameters. All simulations were performed at temperature T = 298.15 K, the solvent and protein dielectric constants were ε_s = 78 and ε_p = 4, respectively. We used a salt concentration of 50 mM as per,[36] which corresponds to an inverse Debye length κ = 0.07374. A variable time step with a minimum of 2 ps is used. At each time step, the system is solved with a polarization cutoff r_{polcut} = 10 Å, and a force cutoff of r_{fcut} = 100 Å. All spheres within a separation distance of r_{polcut} from an external sphere undergo mutual polarization of $\boldsymbol{H}^{(I,k)}$ and $\tilde{\nabla}_I H_{nm}^{(I,k)}$ for two iterative cycles. All multipole and gradient polarization are performed at pole order p = 10. Each sphere surface is discretized into M_p = 1000 points. At each time step, all molecules are propagated using the same Brownian dynamics algorithm described. All simulations were performed on a single processor on an Intel(R) Xeon(R) CPU 2.27 GHz processor with 24GB of physical memory.

3. RESULTS

Northrup-Alison-McCammon (NAM) Methodology. We first compute the bimolecular rate of association of barnase and barstar using the NAM method under the PB-SAM model. Prior to simulation, each protein's self-polarization multipoles are precomputed. During the actual simulation, barnase is fixed at the origin, while barstar is positioned 100 Å away and allowed to move with respect to barnase. If the docking criteria are met, the trajectory is considered docked and then terminated. If the center of mobile barstar moves beyond the truncation sphere of radius q = 500 Å from barnase, the docking event fails and the trajectory is again terminated. The docking frequency δ is then the ratio of successful docking events against the total number of trajectories, and the intrinsic bimolecular collision rate is then calculated as

$$k = \frac{k(b)\delta}{1 - (1 - \delta)k(b)/k(q)} \tag{23}$$

where $k(b)$ and $k(q)$ are rates at which a molecule B starting at infinity reaches $r = b$ and $r = q$, respectively, and which can be evaluated analytically from the Smoluchowski rate equation

Table 2. Bimolecular Rates of Association for Barnase and Barstar[a]

					pseudo-first-order values from fitting			
N_A	barnase [M]	N_B	barstar [M]	δ	k' [ns^{-1}]	t_d [ns]	R^2	k [M^{-1} s^{-1}]
1	5.068×10^{-5}	1	5.068×10^{-5}	22/10531	N/A	N/A	N/A	$6.21 \pm 0.28 \times 10^{7}$
124	6.284×10^{-3}	1	5.068×10^{-5}	8/500	$5.540 \pm 0.271 \times 10^{-4}$	3.524	0.989	$8.82 \pm 0.43 \times 10^{7}$
1	5.068×10^{-5}	124	6.284×10^{-3}	9/500	$4.679 \pm 0.248 \times 10^{-4}$	2.027	0.977	$7.45 \pm 0.39 \times 10^{7}$

[a]The first row is the kinetic rate calculated using the NAM method[38] in which interprotein interactions are not represented. The next two entries correspond to the evaluation of a pseudo-first-order rate constant in which either barnase or barstar is in excess of the other protein. δ is the ratio of the number of successful docking events relative to the number of trajectories simulated. The rate constant using NAM is evaluated from eq 23, while the pseudo-first-order rate constant is determined from the fit to mean first passage docking data using eqs 27-29. R^2 is the measure of quality of fit. The experimental rate value is $k = 2.86 \times 10^8$ M^{-1} s^{-1}, and the value calculated by Gabdoulline and Wade[37] is $k = 3.88 \times 10^8$ M^{-1} s^{-1}.

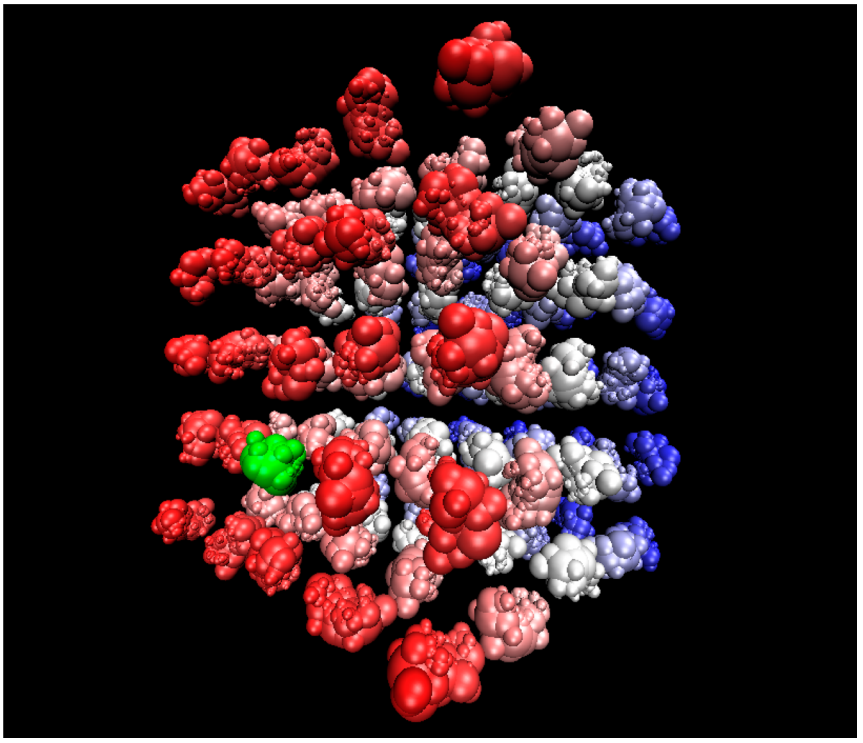

Figure 3. A representative initial configuration for the multimolecular method, showing 124 barnase molecules (red/white/blue spectrum) and 1 barstar (green) placed in a periodic cubic box of length $L = 320$ Å. The starting configuration is generated by placing the geometric center of each molecule on a $5 \times 5 \times 5$ grid, and the molecule type (barnase or barstar) and orientation are then randomly assigned.

$$k(R) = \left[\frac{1}{4\pi(D_{trans})}\int_R^\infty \frac{\exp(U(r)/k_BT)}{r^2}dr\right]^{-1} \quad (24)$$

At a screening length of $\kappa = 0.0737$, the electrostatic interaction $U(r)$ is attenuated to less than 0.01 at the distance $b = 100$ Å and effectively zero at $q = 500$ Å, so the rates can be evaluated as

$$k(b) = 4\pi(D_{trans})b$$
$$k(q) = 4\pi(D_{trans})q \quad (25)$$

We simulated 10,051 trajectories and monitored the number of trajectories that docked according to our docking criteria. We recorded 22 docked trajectories, corresponding to a collision frequency of $2.189 \pm 0.099 \times 10^{-3}$, with error bounds estimated by adding or removing one docking trajectory and recomputing the collision frequency. Using eq 23, we obtained a rate constant of $k = 6.21 \pm 0.28 \times 10^7$ M^{-1} s^{-1}. Our NAM rate is comparable to the experimentally determined value[35] of $k = 2.86 \times 10^8$ M^{-1} s^{-1} and the value calculated by Gabdoulline and Wade[37] of $k = 3.88 \times 10^8$ M^{-1} s^{-1} using NAM and atomistic docking criteria. Our slower NAM rate constant compared to the previous theoretical value is likely due differences in the molecular representations. Regardless, the exact docking definition does not impact our question at hand, which is as follows: given the *same docking criterion*, will the NAM method and the multimolecular simulation produce the same kinetic rate constants.

Rate Constant from Multimolecular Simulation. The second-order rate equation describing the bimolecular association of barnase (A) and barstar (B) is given by

$$\frac{d[AB]}{dt} = k[A][B] \quad (26a)$$

where $[A]$, $[B]$, and $[AB]$ are the concentrations of barnase, barstar, and the docked encounter complex, in units of M, respectively, and k is the intrinsic bimolecular rate constant with unit M^{-1} s^{-1}. We can rewrite the rate equation as

$$\frac{d[AB]}{dt} = k'[B] \tag{26b}$$

where $k' = k[A]$, in units s^{-1}. In the limit of small t, concentrations $[A] \approx [A]_{t=0}$, the initial barnase concentration, so eq 26b assumes the form of a pseudo-first-order rate equation. The pseudo-first-order rate constant k' can be obtained using the first passage time approach. We simulated N independent systems of N_A barnase and N_B barstar molecules and recorded the time taken to form the encounter complex for the first time, t_i, for each system. The fraction of trajectories docked at time t is given by

$$P_{docked}(t) = (\text{No. of systems with } t_i \leq t)/N \tag{27}$$

The pseudo-first-order rate constant k' can be determined from fitting on the plotted data of $P_{docked}(t)$ against t, using

$$P_{docked} = 1 - \exp(-k'(t - \tau_d)) \tag{28}$$

where τ_d is the dead time required for the system to equilibrate. Finally, the bimolecular rate constant was computed from

$$k = k'/[A]_{t=0} \tag{29}$$

For the multimolecular method, a cubic simulation box with periodic boundaries was used. The box length is chosen such that electrostatic forces are sufficiently attenuated after 1 box length, so the minimum image convention can be used, which was 320 Å. Table 2 lists the number of barnase and barstar monomers (N_A and N_B, respectively), in which one simulation $N_A = 124$ and $N_B = 1$ and another simulation in which $N_A = 1$ and $N_B = 124$. For each combination ~500 initial configurations were generated by placing the molecules' geometric centers on a grid at equal separation and randomly assigned the type of molecule (barnase or barstar) based on N_A and N_B and then randomly rotated each molecule. Figure 3 illustrates a representative initial system configuration.

The fitted values of k' and τ_d are also presented in Table 2. Correlation coefficients for fitting the data to the pseudo-first-order rate equation (eq 28) are in the range of 0.977−0.989, providing support that the encounter complex formation can indeed be approximated as a first-order reaction for small t. Standard errors for multimolecular rates were computed using a jack-knife approach: a single docking event was removed, the remaining data was refited to eq 28 to obtain k_{Ji}', and the process was repeated for all N_d docking events. The resulting standard errors in k and k', given by

$$\sigma^2_{Jmean} = \sqrt{(N_d - 1)\sum_{j=1}^{N_d} (k'_{Ji} - k')^2/N_d} \tag{30}$$

are reported in Table 2. To assess convergence, we monitored the fit quality (through correlation coefficients R^2) and k' as we include successively longer docking times into the fit (Supporting Information Figures S1(a)-(b)). We confirmed convergence by observing (i) final R^2 values have converged to 0.38% (for $N_A = 124{:}N_B = 1$) and 1.00% (for $N_A = 1{:}N_B = 124$), and (ii) final k' values have converged to 3.52% (for $N_A = 124{:}N_B = 1$) and 0.87% (for $N_A = 1{:}N_B = 124$). The rates calculated, 7.45×10^7 M^{-1} s^{-1} and 8.82×10^7 M^{-1} s^{-1}, are still within the same order of magnitude compared to experimental and previous *in silico* NAM rates; however, the rate constants from the multimolecular simulation are clearly 15−30% faster. Since both rate calculation methods used exactly the same protein models, force field, and docking definition, the difference in rate constant can only arise from the differences in protein concentration.

4. CONCLUSION

We have extended our semianalytical PB-SAM method for solving the linearized Poisson−Boltzmann equation by presenting expressions for computing the forces and torques on the fly that account for both self-and full mutual polarization effects. We have applied the PB-SAM method to model the systematic force in a Brownian dynamics simulation to study the diffusion-limited association of barnase and barstar under crowding conditions.

We demonstrated that the traditional method of computing bimolecular rate constants using the Smolouchowski-based NAM method,[38] which neglects intraspecies interaction, underestimates the rate constant by ~15−30%. Nonetheless, our association rate constants show modest enhancement under crowding conditions that are in line with experiments that have used both large agents such as PEG or small crowders such as ethylene glycol in which influence on barnase and barstar association rates were also found to be small.[3,4] The common explanation for the marginally faster rate constant using the multimolecular method is that the slowed diffusion of protein molecules in general is balanced against the intraspecies electrostatic repulsion and steric hindrance that effectively reduces the available diffusion space to speed up the interspecies encounter. In this particular case of barnase and barstar under pseudo-first-order rate conditions, the interacting protein in excess is behaving no differently than a steric crowder that are represented by excluded volume spheres.[2]

The PB-SAM approach combined with Brownian dynamics simulated under periodic boundary conditions provides a new methodological approach to systematically studying the effects of complex *interactions* between crowders and target proteins on kinetics and mechanism of protein−protein association. Future improvements would include improved parallelization, hydrodynamic forces, and incorporation into a community simulation code.

■ ASSOCIATED CONTENT

Supporting Information

We have supplied a summary of the analytical and numerical re-expansion operations and convergence of the rate equations with longer simulation times and docking events. This material is available free of charge via the Internet at http://pubs.acs.org.

■ AUTHOR INFORMATION

Corresponding Author

*E-mail: thg@berkeley.edu.

Present Address

[⊥]Department of Systems and Comp. Bio., Albert Einstein College of Medicine, 1300 Morris Park Avenue, Bronx, NY 10461.

Notes

The authors declare no competing financial interest.

■ REFERENCES

(1) McGuffee, S. R.; Elcock, A. H. Diffusion, crowding & protein stability in a dynamic molecular model of the bacterial cytoplasm. *PLoS Comput. Biol.* **2010**, *6*, e1000694.

(2) Qin, S.; Cai, L.; Zhou, H.-X. A method for computing association rate constants of atomistically represented proteins under macromolecular crowding. *Phys. Biol.* **2012**, *9*, 066008.

(3) Phillip, Y.; Kiss, V.; Schreiber, G. Protein-binding dynamics imaged in a living cell. *Proc. Natl. Acad. Sci. U.S.A.* **2012**, *109*, 1461−1466.
(4) Phillip, Y.; Sherman, E.; Haran, G.; Schreiber, G. Common crowding agents have only a small effect on protein-protein interactions. *Biophys. J.* **2009**, *97*, 875−885.
(5) Lu, B. Z.; Zhou, Y. C.; Holst, M. J.; McCammon, J. A. Recent progress in numerical methods for the Poisson-Boltzmann equation in biophysical applications. *Comm. Comp. Phys.* **2008**, *3*, 973−1009.
(6) Kirkwood, J. G. Theory of solutions of molecules containing widely separated charges with special application to zwitterions. *J. Chem. Phys.* **1934**, *2*, 351−362.
(7) Phillies, G. D. Effects of intermacromolecular interactions on diffusion 0.1. 2-component solutions. *J. Chem. Phys.* **1974**, *60*, 976−982.
(8) Phillies, G. D. Effects of intermacromolecular interactions on diffusion 0.2. 3-component solutions. *J. Chem. Phys.* **1974**, *60*, 983−989.
(9) Sader, J. E.; Lenhoff, A. M. Electrical double-layer interaction between heterogeneously charged colloidal particles: a superposition formulation. *J. Colloid Interface Sci.* **1998**, *201*, 233−243.
(10) Mcclurg, R. B.; Zukoski, C. F. The electrostatic interaction of rigid, globular proteins with arbitrary charge distributions. *J. Colloid Interface Sci.* **1998**, *208*, 529−542.
(11) Fenley, A. T.; Gordon, J. C.; Onufriev, A. An analytical approach to computing biomolecular electrostatic potential. I. Derivation and analysis. *J. Chem. Phys.* **2008**, *129*, 075101.
(12) Lotan, I.; Head-Gordon, T. An analytical electrostatic model for salt screened interactions between multiple proteins. *J. Chem. Theory Comput.* **2006**, *2*, 541−555.
(13) Baker, N. A.; Sept, D.; Joseph, S.; Holst, M. J.; McCammon, J. A. Electrostatics of nanosystems: Application to microtubules and the ribosome. *Proc. Natl. Acad. Sci. U.S.A.* **2001**, *98*, 10037−10041.
(14) Nicholls, A.; Honig, B. A rapid finite-difference algorithm, utilizing successive over-relaxation to solve the Poisson-Boltzmann equation. *J. Comput. Chem.* **1991**, *12*, 435−445.
(15) Rocchia, W.; Alexov, E.; Honig, B. Extending the applicability of the nonlinear Poisson-Boltzmann equation: Multiple dielectric constants and multivalent ions. *J. Phys. Chem. B* **2001**, *105*, 6507−6514.
(16) Chen, L.; Holst, M. J.; Xu, J. C. The finite element approximation of the nonlinear Poisson-Boltzmann equation. *Siam J. Numer. Anal.* **2007**, *45*, 2298−2320.
(17) Holst, M.; Baker, N.; Wang, F. Adaptive multilevel finite element solution of the Poisson-Boltzmann equation I. Algorithms and examples. *J. Comput. Chem.* **2001**, *22*, 475−475.
(18) Zhou, Z. X.; Payne, P.; Vasquez, M.; Kuhn, N.; Levitt, M. Finite-difference solution of the Poisson-Boltzmann equation: Complete elimination of self-energy. *J. Comput. Chem.* **1996**, *17*, 1344−1351.
(19) Cai, Q.; Wang, J.; Zhao, H.-K.; Luo, R. On removal of charge singularity in Poisson-Boltzmann equation. *J. Chem. Phys.* **2009**, *130*, 145101.
(20) Geng, W.; Yu, S.; Wei, G. Treatment of charge singularities in implicit solvent models. *J. Chem. Phys.* **2007**, *127*, 114106.
(21) Zhou, Z.; Payne, P.; Vasquez, M.; Kuhn, N.; Levitt, M. Finite-difference solution of the Poisson-Boltzmann Equation: Complete elimination of self-energy. *J. Comput. Chem.* **1996**, *11*, 1344−1351.
(22) Yu, S.; Wei, G. Three-dimensional matched interface and boundary (MIB) method for treating geometric singularities. *J. Comput. Phys.* **2007**, *227*, 602−632.
(23) Yu, S.; Zhou, Y.; Wei, G. Matched interface and boundary (MIB) method for elliptic problems with sharp-edged interfaces. *J. Comput. Phys.* **2007**, *224*, 729−756.
(24) Gilson, M. K.; Davis, M. E.; Luty, B. A.; McCammon, J. A. Computation of electrostatic forces on solvated molecules using the Poisson-Boltzmann equation. *J. Chem. Phys.* **1993**, *97*, 3591−3600.
(25) Im, W.; Beglov, D.; Roux, B. Continuum solvation model: computation of electrostatic forces from numerical solutions to the Poisson-Boltzmann equation. *Comput. Phys. Commun.* **1998**, *111*, 59−75.
(26) Davis, M. E.; Mccammon, J. A. Electrostatics in biomolecular structure and dynamics. *Chem. Rev.* **1990**, *90*, 509−521.
(27) Bordner, A. J.; Huber, G. A. Boundary element solution of the linear Poisson-Boltzmann equation and a multipole method for the rapid calculation of forces on macromolecules in solution. *J. Comput. Chem.* **2003**, *24*, 353−367.
(28) Boschitsch, A. H.; Fenley, M. O.; Zhou, H. X. Fast boundary element method for the linear Poisson-Boltzmann equation. *J. Phys. Chem. B* **2002**, *106*, 2741−2754.
(29) Juffer, A. H.; Botta, E. F. F.; Vankeulen, B. A. M.; Vanderploeg, A.; Berendsen, H. J. C. The electric-potential of a macromolecule in a solvent - a fundamental approach. *J. Comput. Phys.* **1991**, *97*, 144−171.
(30) Zauhar, R. J.; Morgan, R. S. A new method for computing the macromolecular electric-potential. *J. Mol. Biol.* **1985**, *186*, 815−820.
(31) Zhou, H. X. Boundary-element solution of macromolecular electrostatics - interaction energy between 2 proteins. *Biophys. J.* **1993**, *65*, 955−963.
(32) Lu, B. Z.; McCammon, J. A. Improved boundary element methods for Poisson-Boltzmann electrostatic potential and force calculations. *J. Chem. Theory Comput.* **2007**, *3*, 1134−1142.
(33) Lu, B.; Cheng, X.; Huang, J.; McCammon, J. A. AFMPB: An adaptive fast multipole, Poisson-Boltzmann solver for calculating electrostatics in biomolecular systems. *Comput. Phys. Commun.* **2010**, *181*, 1150−1160.
(34) Yap, E.-H.; Head-Gordon, T. A new and efficient Poisson-Boltzmann solver for interaction of multiple proteins. *J. Chem. Theory Comput.* **2010**, *6*, 2214−2224.
(35) Schreiber, G.; Fersht, A. R. Rapid, electrostatically assisted association of proteins. *Nat. Struct. Biol.* **1996**, *3*, 427−431.
(36) Gabdoulline, R. R.; Wade, R. C. Simulation of the diffusional association of Barnase and Barstar. *Biophys. J.* **1997**, *72*, 1917−1929.
(37) Gabdoulline, R. R.; Wade, R. C. Biomolecular diffusional association. *Curr. Opin. Struct. Biol.* **2002**, *12*, 204−213.
(38) Northrup, S.; Allison, S.; McCammon, J. A. Brownian dynamics simulation of diffusion-influenced bimolecular reactions. *J. Chem. Phys.* **1984**, *80*, 1517−1524.
(39) Rakhmanov, E.; Saff, E.; Zhou, Y. Minimal discrete energy on the sphere. *Math. Res. Lett.* **1994**, *1*, 647−662.
(40) Ermak, D. L.; McCammon, J. A. Brownian dynamics with hydrodynamic interactions. *J. Chem. Phys.* **1978**, *69*, 1352−1360.
(41) Buckle, A. M.; Schreiber, G.; Fersht, A. R. Protein-protein recognition: crystal structural analysis of a barnase-barstar complex at 2.0-A resolution. *Biochemistry* **1994**, *33*, 8878−8889.
(42) Shindyalov, I. N.; Bourne, P. E. Protein structure alignment by incremental combinatorial extension (CE) of the optimal path. *Protein Eng.* **1998**, *11*, 739−747.
(43) Dolinsky, T. J.; Czodrowski, P.; Li, H.; Nielsen, J. E.; Jensen, J. H.; Klebe, G.; Baker, N. A. PDB2PQR: expanding and upgrading automated preparation of biomolecular structures for molecular simulations. *Nucleic Acids Res.* **2007**, *35*, W522−W525.
(44) Dolinsky, T. J.; Nielsen, J. E.; McCammon, J. A.; Baker, N. A. PDB2PQR: an automated pipeline for the setup of Poisson-Boltzmann electrostatics calculations. *Nucleic Acids Res.* **2004**, *32*, W665−W667.
(45) Wang, J. M.; Cieplak, P.; Kollman, P. A. How well does a restrained electrostatic potential (RESP) model perform in calculating conformational energies of organic and biological molecules? *J. Comput. Chem.* **2000**, *21*, 1049−1074.
(46) Li, H.; Robertson, A. D.; Jensen, J. H. Very fast empirical prediction and interpretation of protein pKa values. *Proteins* **2005**, *61*, 704−721.
(47) Sanner, M. F.; Olson, A. J.; Spehner, J. C. Reduced surface: An efficient way to compute molecular surfaces. *Biopolymers* **1996**, *38*, 305−320.